Full-Wave Modeling of Buried Pipe Detection with Low-Frequency Ground-Penetrating Radar

D. Caratelli, A. Yarovoy, and L. P. Ligthart
Delft University of Technology, International Research Centre for Telecommunications and Radar
Mekelweg 4, 2628 CD, Delft, the Netherlands
d.caratelli@tudelft.nl

***Abstract*—In this paper, the full-wave analysis of electromagnetic sensing of buried pipes with ground-penetrating radar (*GPR*) in realistic scenarios is presented. *GPR* uses resistively loaded wideband dipole antennas operating in the frequency band from 100 *MHz* to 1 *GHz*. To this end, a locally conformal finite-difference time-domain (*FDTD*) technique, useful to model losses in the soil, and the presence of ground-embedded inhomogeneities with arbitrary shape and material parameters, is adopted. Emphasis is put on the investigation of the antenna pair performance for different *Tx–Rx* separations and elevations over the ground, as well as on the analysis of scattering from buried dielectric and metallic pipes. Furthermore, a frequency-independent equivalent circuit suitable for *CAD* is provided to facilitate the design of the *RF* front-end of ground-penetrating radars, and the methodology to derive relevant circuital parameters is discussed in detail.**

***Index Terms*—Antenna mutual coupling, ground-penetrating radar (*GPR*), finite-difference time-domain technique (*FDTD*), frequency-independent equivalent circuit.**

I. Introduction

Ground-penetrating radar (*GPR*) technology finds applications in many areas such as geophysical prospecting, archeology, civil engineering, environmental engineering, and defense applications as a noninvasive sensing tool [1]-[3]. One key component in any *GPR* system is the receiver/transmitter antenna. Desirable features for *GPR* antennas include efficient radiation of ultra-wideband pulses into the ground, good impedance matching over the operational frequency band, and small size. As the attenuation of radio waves in geophysical media increases with frequency [4], [5], ground-penetrating radars typically operate at frequencies below 1 *GHz* [6]. For either impulse [4] or stepped-frequency continuous-wave applications [7], the wider the frequency range, the better the range resolution of the radar. Continuous wave multi-frequency radars are advantageous over impulse radars in coping with dispersion of the medium, the noise level at the receiver end, and the controllability of working frequency. It requires, however, mutual coupling between the transmit (*Tx*) and receive (*Rx*) antennas, which determines the dynamic range of the sys-tem, to be kept as small as possible [8].

In this paper, the full-wave analysis of electromagnetic coupling mechanisms between resistively loaded wideband dipole antennas operating in realistic *GPR* scenarios is carried out. To this end, a locally conformal finite-difference time-domain (*FDTD*) technique, useful to accurately model electromagnetic structures having complex geometry, is adopted [9], [10]. Such a scheme, necessary to improve the numerical accuracy of the conventional *FDTD* algorithm [11], [12], by avoiding staircase approximation, is based on the definition of effective material parameters [13], suitable to describe the geometrical and electrical characteristics of the structure under analysis. By doing so, the losses in the soil, as well as the presence of ground-embedded inhomogeneities with arbitrary shape and material parameters, are properly taken into account. Emphasis is devoted to the investigation of the antenna pair performances for different *Tx–Rx* separations and elevations over the ground, as well as on scattering from buried dielectric and metallic pipes. Novelty of the analysis lies in the fact that at the lowest operational frequency both the receive antenna and a pipe are situated in the near-field, whilst at the highest operational frequency only the far field is playing the role. The obtained numerical results provide a physical insight into the underlying mechanisms of subsurface diffraction and antenna mutual coupling processes. This information in turn can be usefully employed to optimize the performance of detection algorithms in terms of clutter rejection.

Finally, a frequency-independent equivalent circuit model of the considered antenna pair, suitable for software *CAD* tools, is provided in order to facilitate the design of the *RF* front-end of a ground-penetrating radar. The procedure employed to extract the equivalent circuit is based on a heuristic modification of the Cauer's network synthesis technique [14], useful to model metal, dielectric and radiation losses.

II. The EM Field Prediction Model

The analysis and design of wideband antennas for *GPR* applications has required the development of a specific yet general computational tool useful to analyze electromagnetic structures having complex geometrical and electrical characteristics, using the locally conformal *FDTD* scheme presented in [9], [10]. Such a scheme is needed to accurately model ohmic and radiation losses avoiding the staircase approximation [11], [12] of the geometry and improving the numerical accuracy of the conventional *FDTD* algorithm. To take into account all physical phenomena occuring in the structure under analysis, it has been necessary to evaluate the field distribution in dielectric, as well as metallic regions. To this purpose, each of these regions has been modeled by

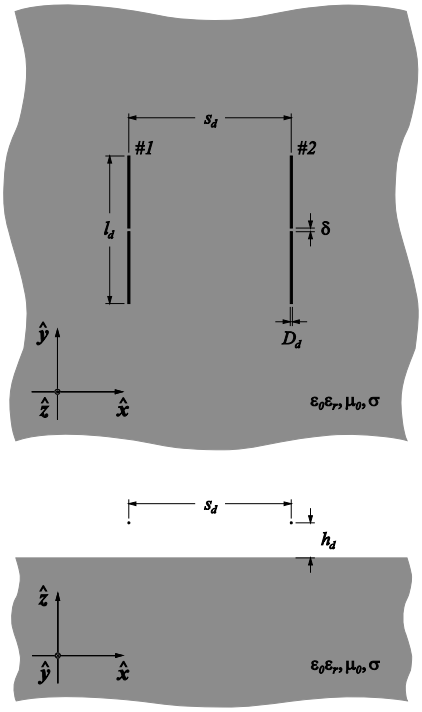

Fig. 1. Top and cross-sectional view of a resistively loaded dipole antenna pair located above a lossy homogeneous half space. Structure characteristics: $l_d = 40\,cm$, $D_d = 5\,mm$, $\delta = 2.5\,mm$, $\varepsilon_r = 6$, $\sigma = 15\,mS/m$. The reference system used to express the field quantities is also shown.

means of the relevant effective permittivity and electrical conductivity parameters.

III. The Full-Wave Antenna Modeling

It is our intention to focus the attention on the full-wave analysis of a resistively loaded dipole antenna pair located above a ground modeled as a lossy homogeneous half-space having relative permittivity $\varepsilon_r = 6$ and electrical conductivity $\sigma = 15\,mS/m$. The geometry of the structure is depicted in Figure 1.

The dipoles are denoted as dipole #1 and dipole #2, respectively. In this configuration, dipole #1 is driven by a delta-gap voltage source with internal resistance $R_0 = 300\,\Omega$, whereas dipole #2 is closed on a matched load having impedance $Z_L = R_0$. To properly enlarge the antenna bandwidth, thus reducing late-time ringing phenomena, a continuous resistive loading, having Wu-King-like profile [3], [15], [16]

$$\sigma_d(y) = \sigma_0\left(1 - \frac{2|y|}{l_d}\right), \tag{1}$$

has been applied to the flairs of the considered radiators. In (1), σ_0 denotes the electrical conductivity value at the input terminals of the antennas ($y = 0$), and $l_d = 40\,cm$ is the length of each dipole, assumed to have diameter $D_d = 5\,mm$. In particular, σ_0 has been determined by means of a specific parametric analysis. In this way, the optimal value

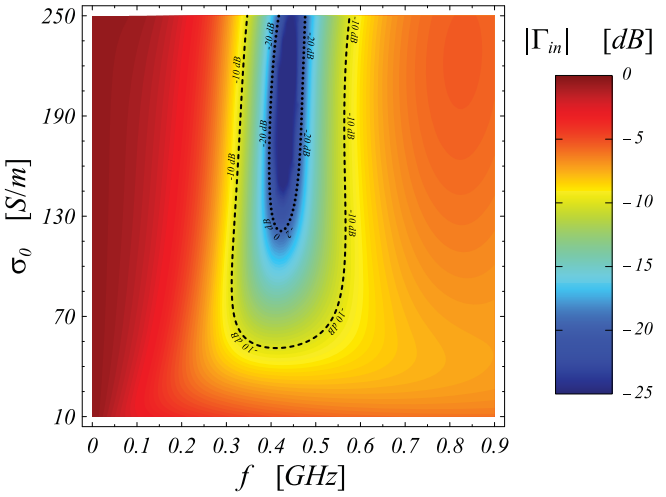

Fig. 2. Frequency behavior of the individual antenna input reflection coefficient for different loading profiles. The antenna is assumed to be elevated $h_d = 3\,cm$ over the ground.

$\sigma_0 = \sigma_{opt} \simeq 200\,S/m$, resulting in a fractional bandwidth $FBW \simeq 51\%$ centered on the resonant frequency $f_r \simeq 450\,MHz$, has been found (see Figure 2).

The *FDTD* characterization of the structure has been

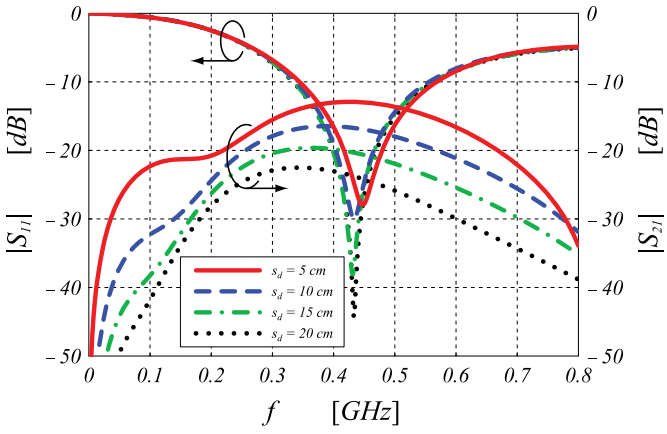

(*a*)

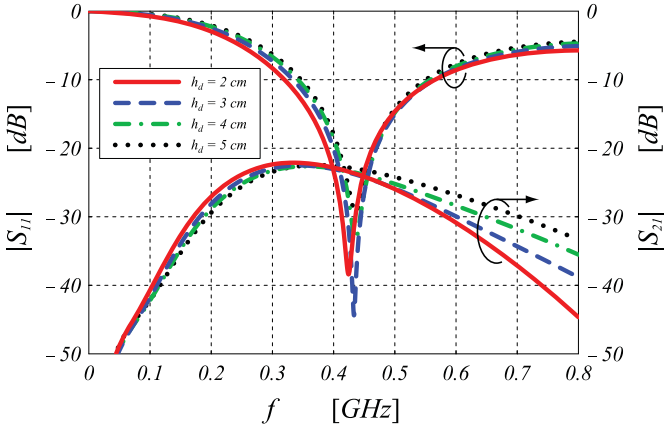

(*b*)

Fig. 3. Frequency behavior of the scattering parameters of the dipole pair for different *Tx–Rx* separations (*a*) and antenna elevations (*b*) over the ground modeled as a lossy homogeneous half-space with electrical properties $\varepsilon_r = 6$, and $\sigma = 15\,mS/m$.

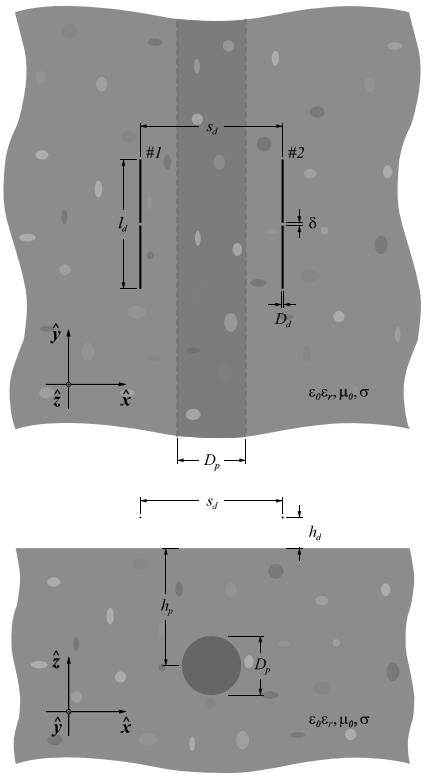

Fig. 4. Top and cross-sectional view of a resistively loaded dipole antenna pair located above a lossy inhomogeneous ground, where an infinitely long pipe is buried. Structure characteristics: $l_d = 40\,cm$, $D_d = 5\,mm$, $\delta = 2.5\,mm$, $s_d = 20\,cm$, $h_d = 3\,cm$, $D_p = 30\,cm$, $h_p = 40\,cm$.

carried out using a non-uniform computational grid with maximum cell size $\Delta h = \lambda_{\min}/24 = 2.5\,mm$, where $\lambda_{\min} \simeq 6\,cm$ is the wavelength in the ground at the maximum operating frequency $f_{\max} = 1\,GHz$ in the excitation Gaussian signal.

Since the considered structure is reciprocal and symmetrical (see Figure 1), the corresponding scattering matrix $\underline{\mathbf{S}}$ is completely described in terms of the S_{11} and S_{21} parameters, whose evaluation is carried out by feeding the first antenna element, and setting the excitation signal of the second dipole equal to zero. Their frequency behavior is shown in Figure 3. As it appears from Figure 3*a*, the return-loss is slightly affected by the *Tx–Rx* antenna separation that, on the other hand, is primarily responsible for the parasitic coupling level between the radiating elements. The impact of the antenna elevation above the ground has been also analyzed (see Figure 3*b*). It is worth noting that, as h_d decreases, the central resonant frequency of the antenna is shifted down because of the proximity effect of the soil. It has been also found that the ground influence on the S_{21} parameter is remarkable only at high frequencies, where the coupling level between the two radiating elements tends to decrease as the dipoles approach the air-ground interface.

IV. The Radar Detection of Buried Pipes

In this section, emphasis is devoted to the analysis of the dipole antenna pair located above a lossy homogeneous/inhomogeneous material half space where an

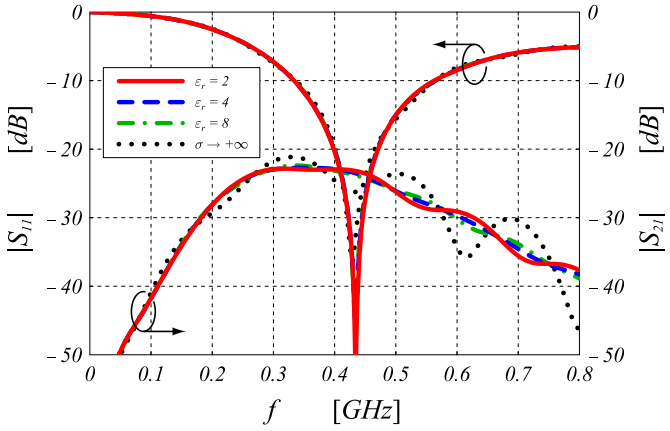

Fig. 5. Frequency behavior of the scattering parameters of the dipole antenna pair for different electrical properties of the buried pipe. Structure characteristics: $l_d = 40\,cm$, $D_d = 5\,mm$, $\delta = 2.5\,mm$, $s_d = 20\,cm$, $h_d = 3\,cm$, $D_p = 30\,cm$, $h_p = 40\,cm$.

infinitely long pipe is buried (see Figure 4). In such configuration, the transmit element of the radar unit emits an electromagnetic pulse that propagates into the ground, where it interacts with the target, modeled as a y −directed circular cylinder having diameter $D_p = 30\,cm$, buried at a depth $h_p = 40\,cm$. This interaction results in a diffracted electromagnetic field which is measured by the receive element of the radar. By changing the location of the radar on the soil interface and recording the output of the receive antenna as function of time (or frequency) and radar location, one obtains the scattering data, which can be processed to get an image of the subsurface.

The parasitic coupling level between transmit and receive antennas is a critical parameter in the design of ground-penetrating radars and satisfactory levels are usually achieved by empirical design methods. Anyway, the prediction of coupling levels already at the design stage enhances structure reliability, while also improving design cycle. To this end, the locally conformal *FDTD* model presented in Section II has been usefully adopted. As it can be noticed in Figure 5, the antenna return-loss parameter S_{11} is not strongly affected by the buried target that, conversely, has a significant impact on

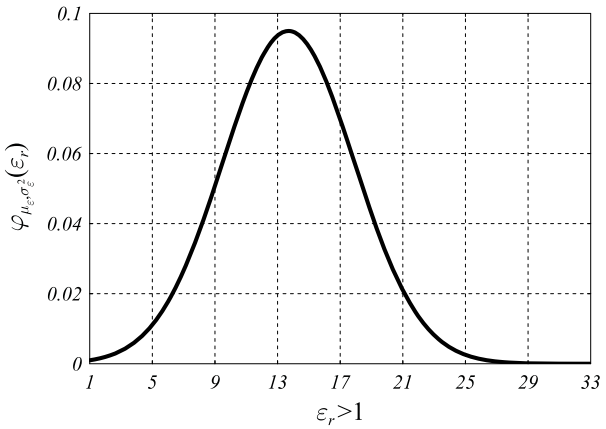

Fig. 6. Gaussian probability distribution of the relative permittivity of ground-embedded inhomogeneities.

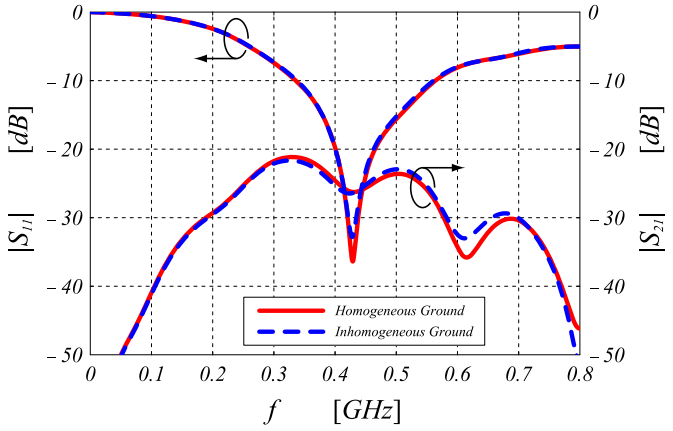

Fig. 7. Effect of the ground inhomogeneities on the frequency behavior of the scattering parameters of the dipole pair. Structure characteristics: $l_d = 40\,cm$, $D_d = 5\,mm$, $\delta = 2.5\,mm$, $s_d = 20\,cm$, $h_d = 3\,cm$.

the frequency behavior of the coupling level between the radiating elements, due to the excitation of subsurface creeping waves resulting in interference processes at the receiver end.

An invariable feature of real-life soils is heterogeneity. Without taking into account the inhomogeneities altering the idealized nature of the considered ground model, it becomes a futile effort to design a complex *GPR* system that will perform well over a real-life soil. To overcome this limitation, a realistic ground model has been developed by simulating small ellipsoidal scatterers embedded in the soil (see Figure 4). The size, location and electrical properties of these inhomogeneities are determined randomly within preset limits. In particular, the maximum dimensions of the scatterers are $a_x = 10\,cm$, $a_y = 10\,cm$, and $a_z = 2\,cm$ in $x-$, $y-$, and $z-$coordinate direction, respectively. In addition, all inhomogeneities have randomly selected values of the relative permittivity according to the following Gaussian probability distribution

$$\varphi_{\mu_\varepsilon,\sigma_\varepsilon^2}(\varepsilon_r) = \frac{1}{\sqrt{2\pi}\,\sigma_\varepsilon} e^{-\frac{(\varepsilon_r-\mu_\varepsilon)^2}{2\sigma_\varepsilon^2}}, \qquad (2)$$

with mean $\mu_\varepsilon = 13.7$, and standard deviation $\sigma_\varepsilon = 4.2$ (see Figure 6). As it appears from Figure 7, the ground-embedded inhomogeneities have a considerable influence on the scattering parameters of the dipole pair at higher frequencies, where the radiated field assumes a quasi-optical behavior, and diffraction processes arising from the interaction with the inhomogeneities tends to be significant, and could mask the detection of the buried target (see Figure 8).

As outlined in [17], the rigorous analysis of the aforementioned subsurface scattering phenomena is very important in order to asses the suitability of detection and imaging algorithms for *GPR* applications in realistic scenarios.

V. Frequency-Independent Equivalent Circuit Model

Typically, electromagnetic field solvers and measurement

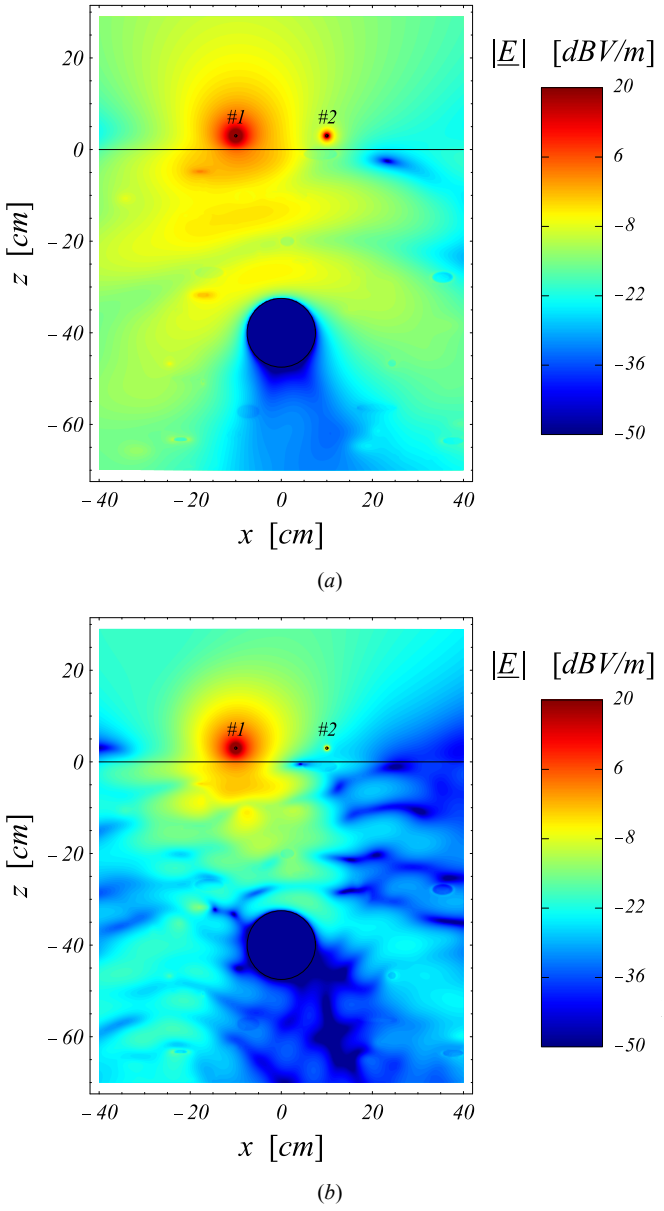

Fig. 8. Spatial distribution of the electric field excited along the vertical cut-plane of the antenna pair elevated over a lossy inhomogeneous ground, where an infinitely long metallic pipe is buried. Structure characteristics: $l_d = 40\,cm$, $D_d = 5\,mm$, $\delta = 2.5\,mm$, $s_d = 20\,cm$, $h_d = 3\,cm$, $D_p = 30\,cm$, $h_p = 40\,cm$. Working frequency: $f = 500\,MHz$ (*a*), $f = 1\,GHz$ (*b*).

systems, such as network analyzers, generate $S-$parameter representations of microwave components and antennas. However, circuit simulators, such as *SPICE*, require conventional equivalent circuits with lumped frequency-independent parameters that can be conveniently modeled within *CAD* software. In view of this, a technique for extracting the equivalent circuit, as well as its electrical parameters, from a given $S-$parameter representation is highly desirable [18].

The procedure employed to extract the equivalent circuit is based on a heuristic modification of the Cauer's network synthesis technique [14]. Resistive elements are introduced to model metal, dielectric, and radiation losses. The scattering matrix $\underline{\mathbf{S}}$ of the antenna pair is modeled by means of an

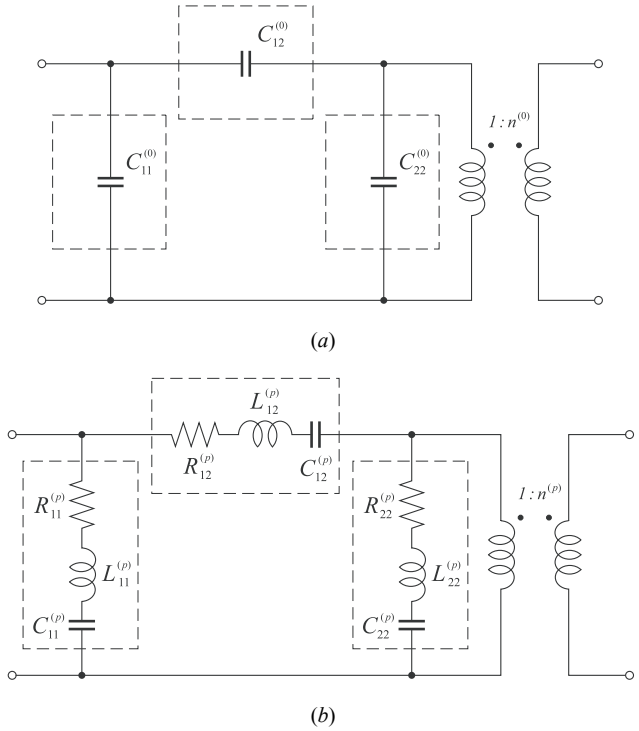

Fig. 9. Frequency-independent equivalent circuit model. Quasi-static (*a*), and $p-th$ high-frequency (*b*) $\pi-$ network. For symmetrical structures the transformation ratio $n^{(p)}$ is equal to ± 1 for each sub-network.

equivalent network composed of shunt $\pi-$ networks as shown in Figure 9, where ideal transformers are to be included in order to guarantee the physical realizability of the network. In particular, RLC $\pi-$ networks are required to properly model the high-frequency resonant phenomena taking place into the structure, whereas the capacitive $\pi-$ network is needed to describe the circuital behavior of the antenna pair in quasi-static regime.

TABLE I
CIRCUITAL PARAMETERS APPEARING IN THE EQUIVALENT CIRCUIT OF THE ANTENNA PAIR.

$C_{11}^{(0)}=C_{22}^{(0)}$	0.579 pF
$C_{21}^{(0)}$	14.562 fF
$n^{(0)}$	+1
$R_{11}^{(1)}=R_{22}^{(1)}$	208.073 Ω
$L_{11}^{(1)}=L_{22}^{(1)}$	0.141 μH
$C_{11}^{(1)}=C_{22}^{(1)}$	1.565 pF
$R_{21}^{(1)}$	1.307 $k\Omega$
$L_{21}^{(1)}$	1.507 μH
$C_{21}^{(1)}$	0.147 pF
$n^{(1)}$	+1
$R_{11}^{(2)}=R_{22}^{(2)}$	322.581 Ω
$L_{11}^{(2)}=L_{22}^{(2)}$	0.092 μH
$C_{11}^{(2)}=C_{22}^{(2)}$	0.235 pF
$R_{21}^{(2)}$	1.838 $k\Omega$
$L_{21}^{(2)}$	1.084 μH
$C_{21}^{(2)}$	0.020 pF
$n^{(2)}$	+1

A simple analysis of the network shown in Figure 9 allows determining the admittance matrix $\underline{\mathbf{Y}}^{eq}$ of the equivalent circuit. Then, the corresponding scattering matrix $\underline{\mathbf{S}}^{eq}$ can be easily computed as follows

$$\underline{\mathbf{S}}^{eq}=\left(\underline{\mathbf{I}}-\underline{\hat{\mathbf{Y}}}^{eq}\right)\cdot\left(\underline{\mathbf{I}}+\underline{\hat{\mathbf{Y}}}^{eq}\right)^{-1}, \tag{3}$$

where $\underline{\mathbf{I}}$ is the identity matrix, and

$$\underline{\hat{\mathbf{Y}}}^{eq}=R_0\underline{\mathbf{Y}}^{eq}, \tag{4}$$

R_0 denoting the reference resistance at the input ports of the transmit and receive antennas.

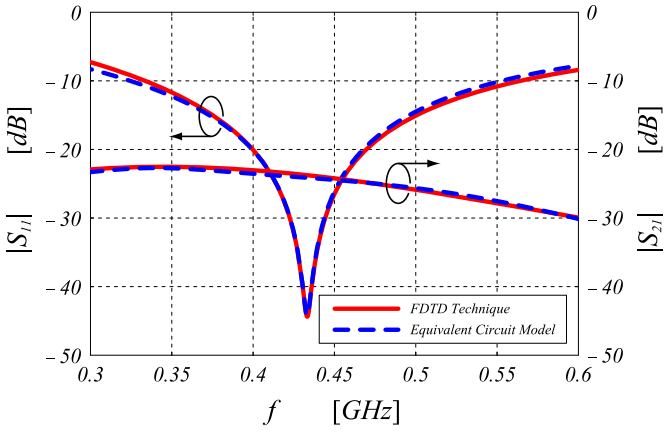

Fig. 10. Magnitude of the scattering parameters of the dipole pair versus frequency. A good agreement between the *FDTD* numerical results and those obtained by means of the equivalent circuit model is observed. Structure characteristics: $l_d=40\,cm$, $D_d=5\,mm$, $\delta=2.5\,mm$, $s_d=20\,cm$, $h_d=3\,cm$.

The synthesis procedure is based on an iterative non-linear fitting procedure [19] aimed to minimize, across a specific frequency band B, the mean-square error functional

$$e_B\left(R_{ij}^{(p)},L_{ij}^{(p)},C_{ij}^{(p)}\right)= \\ =\sqrt{\int_B\left\|\underline{\mathbf{S}}^{FDTD}(f)-\underline{\mathbf{S}}^{eq}\left(f,R_{ij}^{(p)},L_{ij}^{(p)},C_{ij}^{(p)}\right)\right\|^2 df}, \tag{5}$$

$\underline{\mathbf{S}}^{FDTD}$ being the frequency-dependent scattering matrix of the structure computed by means of the locally conformal *FDTD* technique.

In this way, it has been possible to evaluate numerically the circuital parameters, listed in Table I, of the radar unit located above the lossy homogeneous material half space with relative permittivity $\varepsilon_r=6$ and electrical conductivity $\sigma=15\,mS/m$. As shown in Figure 10, only a few resonant $\pi-$ networks are necessary to describe adequately the antenna return-loss and

mutual coupling coefficient in the frequency band of interest.

VI. Conclusion

The full-wave analysis of electromagnetic sensing of buried pipes with *GPR* in realistic scenarios has been carried out. A locally conformal *FDTD* technique, useful to accurately model complex electromagnetic structures as well as ground-embedded inhomogeneities with arbitrary shape and material parameters, has been adopted. Using such scheme, an extensive parametric analysis of the antenna scattering parameters and radiated near-field spatial distribution has been performed for different *Tx–Rx* antenna separations and elevations over the ground, also taking into account the presence of buried metallic and dielectric targets, as well as soil-embedded ellipsoidal inhomogeneities with arbitrary size, location and electrical properties. The obtained numerical results provide a physical insight into the underlying mechanisms of subsurface scattering and antenna mutual coupling processes. Finally, a frequency-independent equivalent circuit, useful to be employed in *CAD* tools, has been derived from the antenna scattering parameters, showing that including the effect of just a few resonant modes yields high numerical accuracy.

VII. Acknowledgment

This research has been done in the framework of *EU*-sponsored project *ORFEUS* (contract number: *FP6-2005-Global-4-036856*).

References

[1] L. Peter Jr., J. D. Young, and J. Daniels, "Ground penetration radar as a subsurface environmental sensing tool," *Proc. IEEE*, vol. 82, pp. 1802–1822, Dec. 1994.

[2] D. Daniels, Ground Penetrating Radar, 2nd ed., IEE Press, 2004.

[3] D. Caratelli, A. Yarovoy, and L. P. Ligthart, "Antennas for ground-penetrating radar applications," Delft University of Technology, the Netherlands, *Tech. Rep. IRCTR–S–032–07*, July 12, 2007.

[4] K. Iizuka, A. P. Freundorfer, K. H. Wu, H. Mori, H. Ogura, and V. Nguyen, "Step-frequency radar," *J. Appl. Phys.*, vol. 56, pp. 2572–2583, 1984.

[5] A. Freundorfer, K. Iizuka, and R. Ramseier, "A method of determining electrical properties of geophysical media," *J. Appl. Phys.*, vol. 55, pp. 218–222, 1984.

[6] D. Caratelli, A. Yarovoy, and L. P. Ligthart, "Design and analysis of antennas for ground-penetrating radar applications," Delft University of Technology, the Netherlands, *Tech. Rep. IRCTR–S–041–07*, Sept. 11, 2007.

[7] R. M. Moray, "Continuous subsurface profiling by impulse radar," *Proc. Eng. Found. Conf. Amer. Soc. Civil Eng.*, pp. 213–232, 1974.

[8] L. Gürel and U. Oguz, "Optimization of the transmitter–receiver separation in the ground-penetrating radar," *IEEE Trans. Antennas Propagat.*, vol. 51, pp. 362–370, Mar. 2003.

[9] D. Caratelli and R. Cicchetti, "A full-wave analysis of interdigital capacitors for planar integrated circuits," *IEEE Trans. Magnetics*, vol. 39, pp. 1598–1601, May 2003.

[10] D. Caratelli, R. Cicchetti, G. Bit-Babik, and A. Faraone, "A perturbed E-shaped patch antenna for wideband WLAN applications," *IEEE Trans. Antennas Propagat.*, vol. 54, pp. 1871–1874, June 2006.

[11] K. S. Yee, "Numerical solution of initial boundary value problems involving Maxwell's equations," *IEEE Trans. Antennas Propagat.*, vol. 14, pp. 302–307, May 1966.

[12] A. Taflove and S. C. Hagness, *Computational Electrodynamics: The Finite-Difference Time-Domain Method*, Artech House, 2000.

[13] N. Kaneda, B. Houshmand, and T. Itoh, "FDTD analysis of dielectric resonators with curved surfaces," *IEEE Trans. Microwave Theory Tech.*, vol. 45, pp. 1645–1649, Sept. 1997.

[14] E. A. Guillemin, *Synthesis of Passive Network: Theory and Methods Appropriate to the Realization and Approximation Problems*, John Wiley, 1965.

[15] J. G. Maloney and G. S. Smith, "A study of transient radiation from the Wu-King resistive monopole – FDTD analysis and experimental measurements," *IEEE Trans. Antennas Propagat.*, vol. 41, pp. 668–676, May 1993.

[16] T. P. Montoya and G. S. Smith, "A study of pulse radiation from several broad-band loaded monopoles," *IEEE Trans. Antennas Propagat.*, vol. 44, pp. 1172–1182, Aug. 1996.

[17] L. Gürel and U. Oguz, "Simulations of ground-penetrating radars over lossy and heterogeneous grounds," *IEEE Trans. Geosci. Remote Sensing*, vol. 39, pp. 1190–1197, June 2001.

[18] I. Timmins and K. Wu, "An efficient systematic approach to model extraction for passive microwave circuits," *IEEE Trans. Microwave Theory Tech.*, vol. 48, pp. 1565–1573, Sept. 2000.

[19] R. Fletcher, *Practical methods of optimization*, John Wiley, 1980.